JOURNAL OF MATERIALS SCIENCE **40** (2005) 5821–5828

Fracture of open- and closed-cell metal foams

P. R. ONCK*, R. VAN MERKERK, A. RAAIJMAKERS, J. TH. M. DE HOSSON
Department of Applied Physics, Materials Science Center and the Netherlands Institute for Metals Research, University of Groningen, Nijenborgh 4, 9747 AG Groningen, The Netherlands

Two closed cell aluminium foams and one open cell nickel-chromium foam were subjected to microstructural characterization, *in situ* fracture tests and fractography. The failure process of the open cell foam was observed to be rather ductile, while that of the closed cell foams was found to be brittle. The ductility was related to the purity of the nickel chromium alloy, resulting in necking to be the dominant source of energy dissipation during failure. The brittleness of the closed cell foams was related to the presence of precipitates and particles in the cell wall microstructure, limiting the amount of plastic dissipation. The embrittling phases were traced back to the alloy composition, viscosity enhancing additions and foaming agent.

1. Introduction

The structural applicability of commercially available metal foams is limited to compressive loading situations, due to their inherent brittleness in tension. Under compressive loading metal foams deform until they reach the densification strain of approximately 80 percent (for a relative density of 0.1). However, they have a tensile failure strain of the order of a few percent and

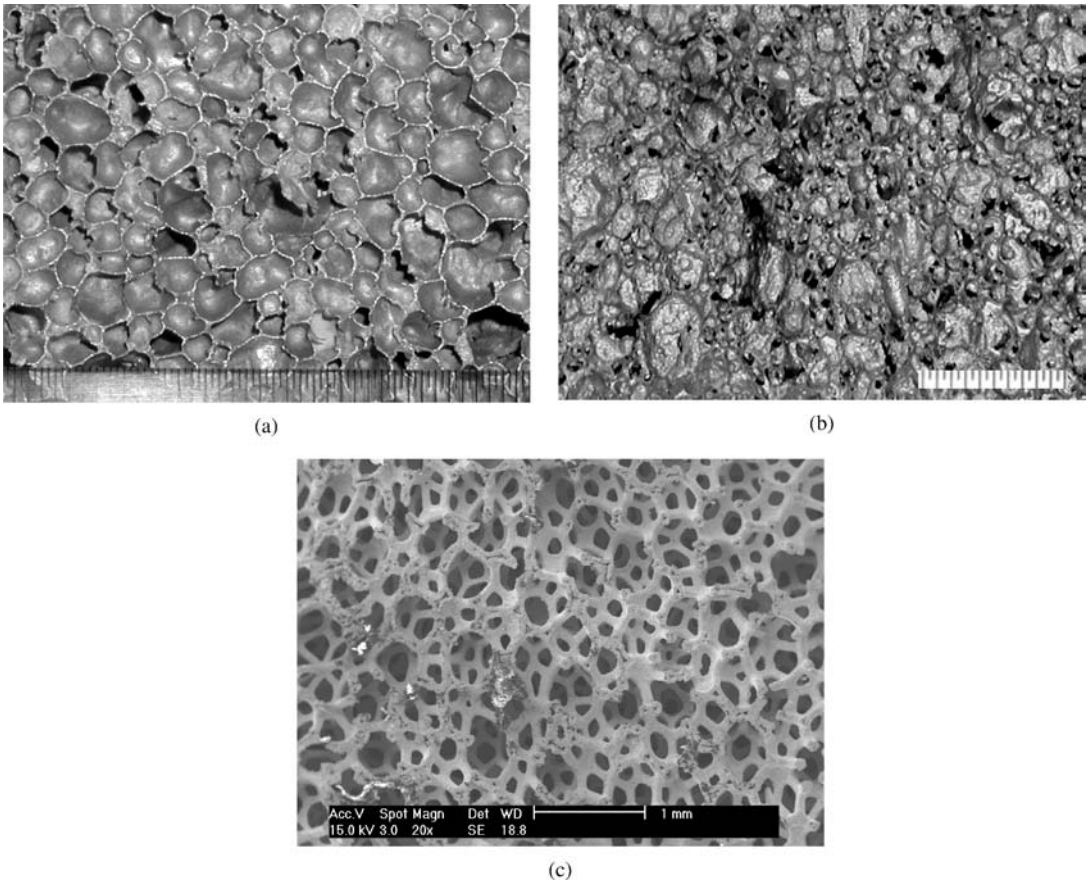

Figure 1 The three foams analyzed. (a) Alporas closed-cell Al foam, manufactured by Shinko Wire Company Ltd, Japan; (b) Cymat closed-cell Al foam, manufactured by Cymat Aluminium Corporation, Canada; (c) Recemat® Metal Foam, manufactured by Recemat International BV, The Netherlands.

*Author to whom all correspondence should be addressed.
0022-2461
DOI: 10.1007/s10853-005-4996-7

sometimes even less than a percent [1]. Similar values for tensile failure strains have been found for fatigue loading [2]. This brittleness is related to the presence of precipitates and particles in the cell wall microstructure, resulting from the specific manufacturing process. In the quest to manufacture foams at minimal cost and with a minimum of morphological imperfections (being the main cause for the knockdown in compressive stiffness and strength [1]), the resulting cell wall microstructure is given lower priority. As a result, embrittling phases are left in the cell walls, resulting from chemical blowing agents and viscosity enhancing ingredients. The aim of this paper is to relate to failure mechanisms in tension to the cellular architecture and cell wall microstructure in order to improve manufacturing procedures leading to tougher foams.

We analyze three metal foams: two closed-cell aluminium foams and one open-cell nickel-chromium foam. The first closed-cell foam is manufactured by Shinko Wire Company Ltd, Japan, tradename Alporas, using a chemical foaming process (see Fig. 1a). The second closed-cell foam is manufactured by Cymat

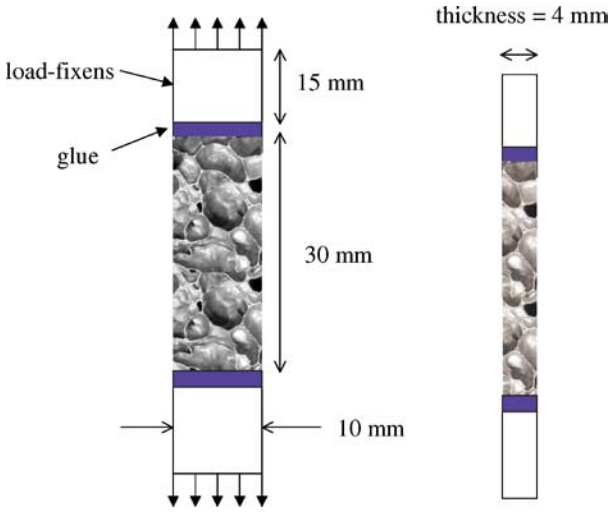

Figure 3 Geometry of the in-situ testing samples of Alporas (and Cymat). Left: front view, right: side view.

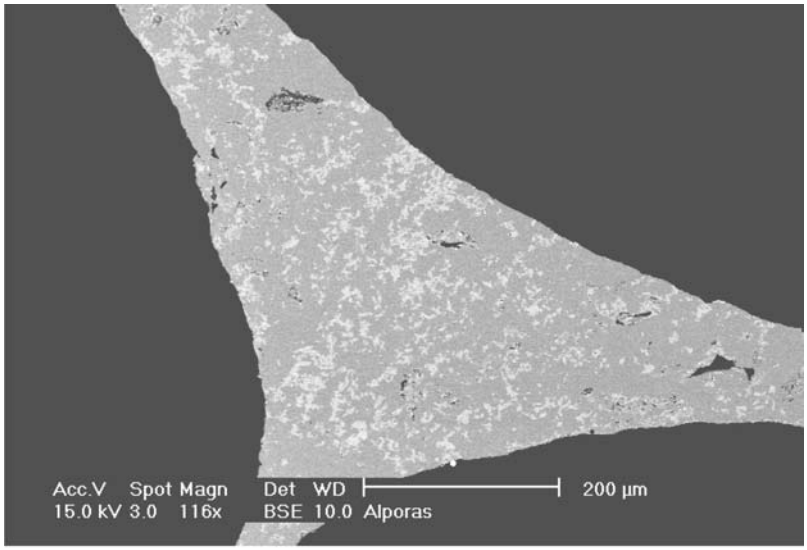

(a)

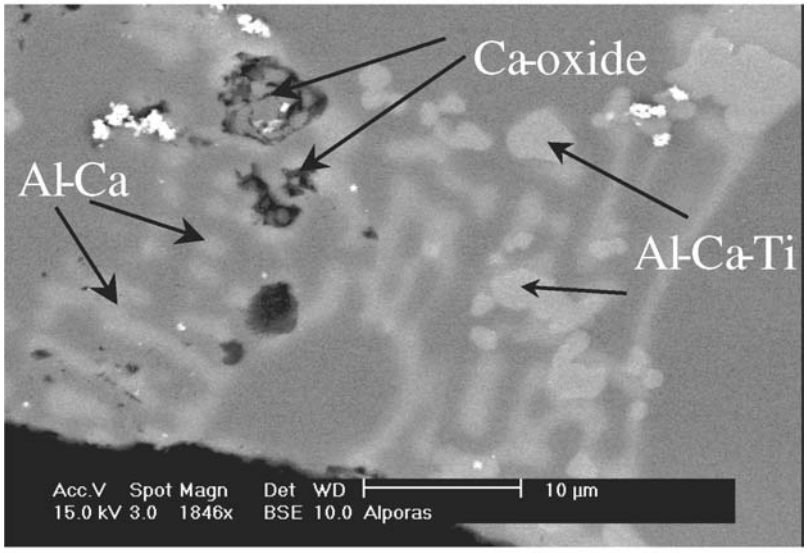

(b)

Figure 2 Cell-wall microstructure of Alporas foam. (a) BSE image of a section through a plateau border. (b) BSE image of the cell wall material.

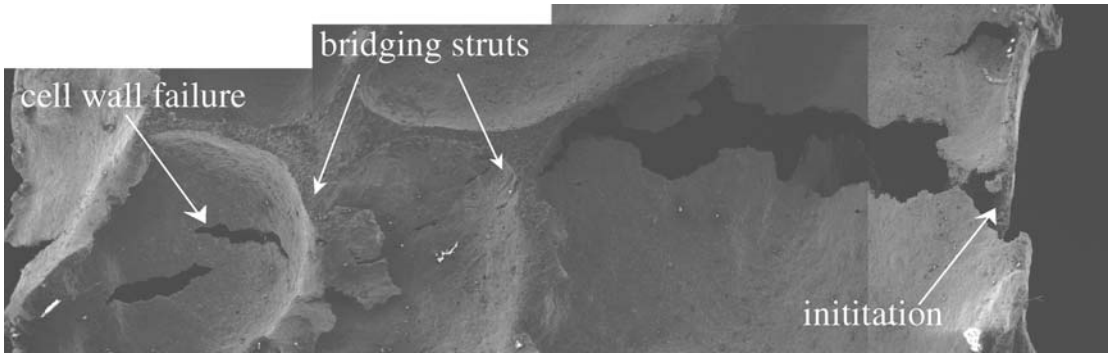

Figure 4 Collection of SEM images spanning the width of the Alporas specimen at the moment prior to final failure. Picture width: 10 mm.

Aluminium Corporation, Canada, named Cymat foam, based on a mechanical foaming process (see Fig. 1b). The third foam is manufactured by Recemat International BV, The Netherlands, product name Recemat® Metal Foam (named Recemat foam hereafter), using metal deposition on a polymer preform (see Fig. 1c). The paper is organized as follows. For each foam the production method is discussed and the resulting microstructure is characterized. Then, in-situ fracture tests are performed on small foam samples, focusing on the in-situ deformation and fracture mechanisms. Finally, the fracture surfaces are analyzed.

2. Alporas

Alporas is produced by a chemical foaming process. First 1.5 wt% Ca is added to the molten aluminium to enhance the viscosity after which 1.6 wt% TiH_2 is added. The titanium hydride decomposes in titanium and hydrogen gas, where the hydrogen gas forms the bubbles (see [1, 11, 12] for more details on manufacturing procedures). Alporas foam is known for its relatively uniform cell size (see Fig. 1a).

2.1. Microstructural characterization

The Alporas foam analyzed here has a relative density in the range 0.08–0.12, a cell size ranging from 1 to 5 mm, a strut thickness of 200–500 μm and a cell wall thickness of 50–200 μm. Fig. 2a shows a BSE image of a section through a plateau border, consisting of a strut with three neighboring cell walls. Secondary phases (light) are dispersed in the aluminum matrix (dark). Fig. 2b shows a magnification of the cell wall material consisting of three different phases identified by EDS: calcium oxides (black), Al-Ca and Al-Ca-Ti precipitates. In a different batch we also found Al-Ca-Ti-Fe particles. These secondary aluminium phases were also found in [3–5]. The calcium oxides were identified to be compounds such as CaO and Al_2CaO_4 [6] or $Al_2Ca_3O_6$ [13], formed during addition of calcium to the aluminium melt in the viscosity enhancement stage of the manufacturing process. By analyzing etched sections of the foam we found that the particles are clustered together and organized around the grain boundaries. The Al-Ca phase is most likely Al_4Ca (conform [3, 5, 13]). The Al-Ca-Ti phase was suggested to be eutectic [4, 5] for which we, however, found no evidence. The grain size was observed to be in the range 30–100 μm.

(a)

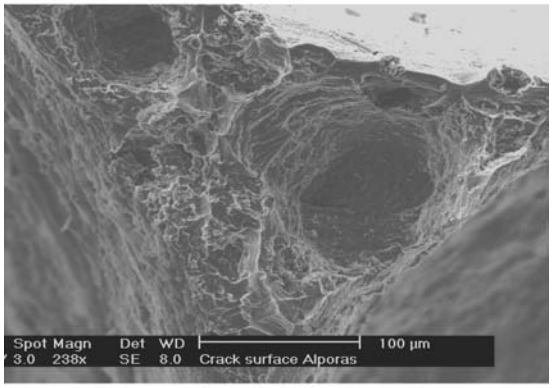

(b)

Figure 5 (a) BSE image of a representative part of the fracture surface showing a ductile region (I) and a brittle region (II). (b) Fracture surface of an Alporas strut showing a large hole.

2.2. *In situ* fracture and fractography

To study the fracture behavior in-situ we tested small samples of Alporas (see Fig. 3), having approximately 3 cells in the width and 1 cell through the thickness, which is clearly not conform the requirements for bulk behavior (at least 7 cell sizes through width and thickness, see [7, 8]). The samples were glued to Al plates (using an expoxy glue) which were mounted in the testing machine. Fig. 4 shows a collection of SEM images spanning the entire width of the specimen at the moment just prior to final failure. Cracking initiates at the right edge of the sample after which the neighboring cell wall progressivity tears. At this stage cracks initiate in the center of neighboring cell walls, oriented perpendicular to the loading direction. Characteristic

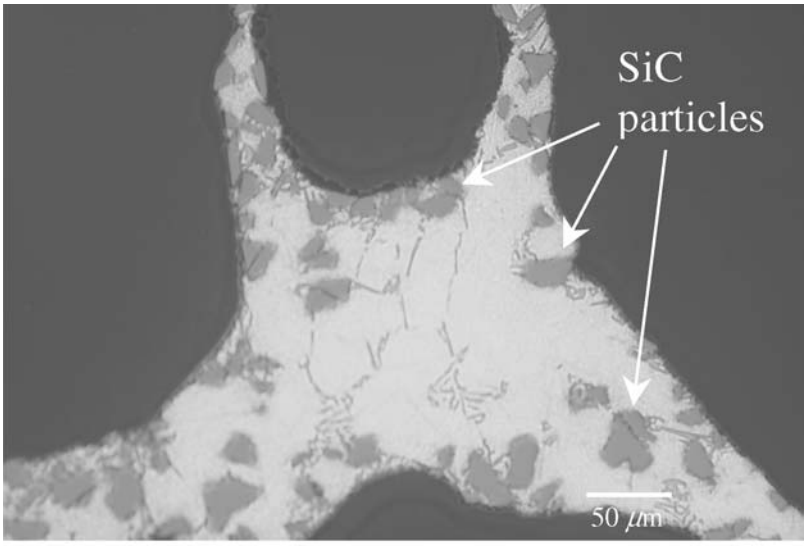

(a)

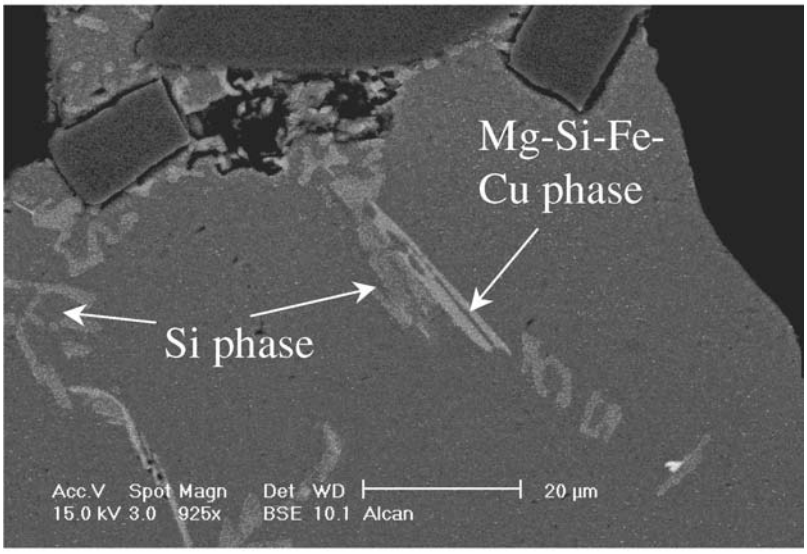

(b)

Figure 6 (a) BSE image of a section of Cymat foam showing the SiC particles. (b) Interdendritic second phase particles.

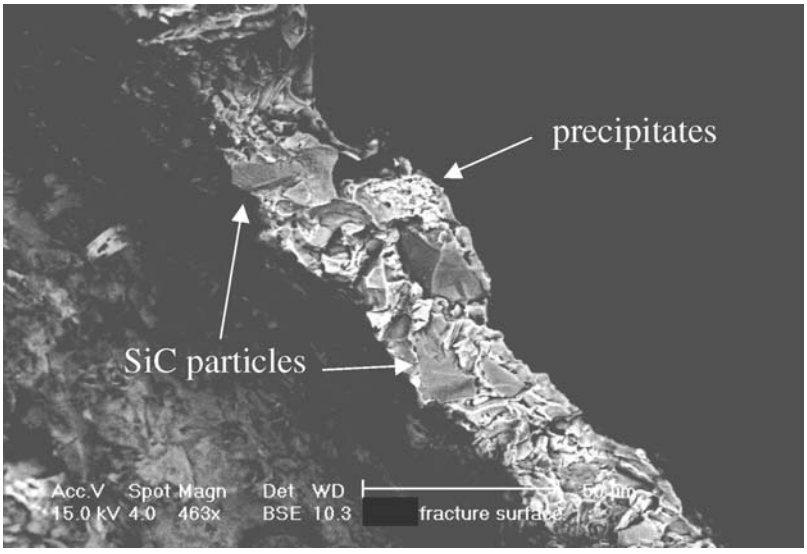

Figure 7 Fracture surface of a Cymat cell wall, showing the SiC particles and precipitates.

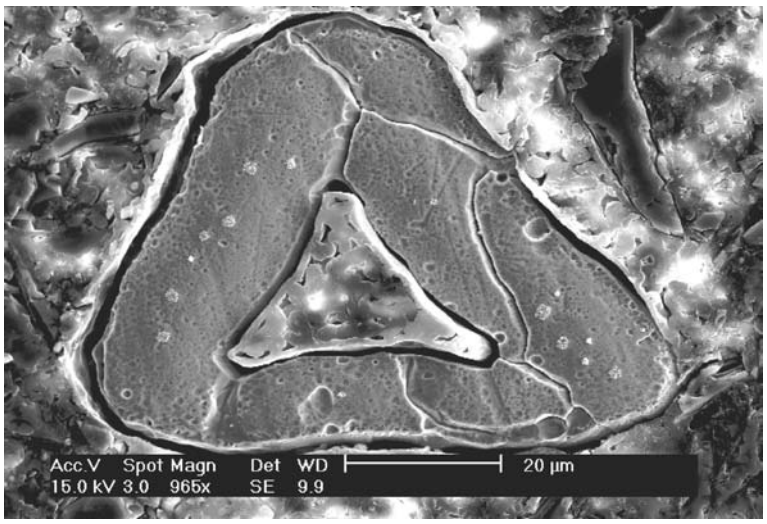

Figure 8 Etched section through a Recemat strut.

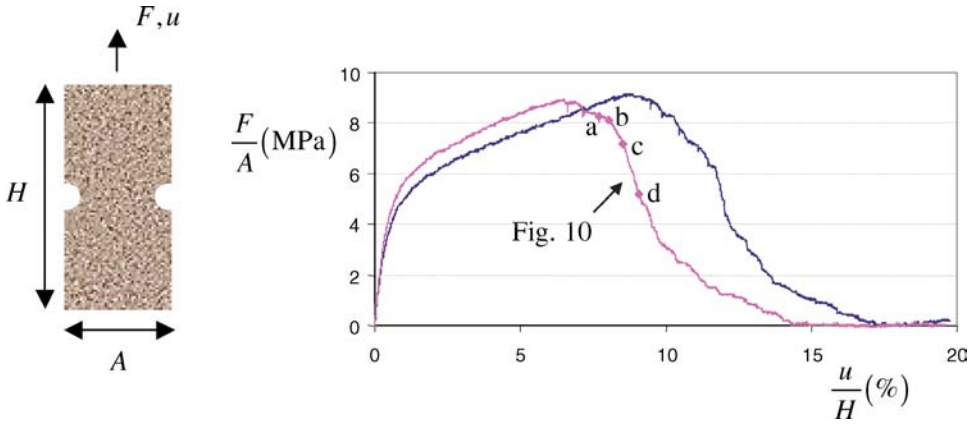

Figure 9 In-situ tensile tests of Recemat foam: Sample geometry (left) and (normalized) force-displacement curves of two tensile tests.

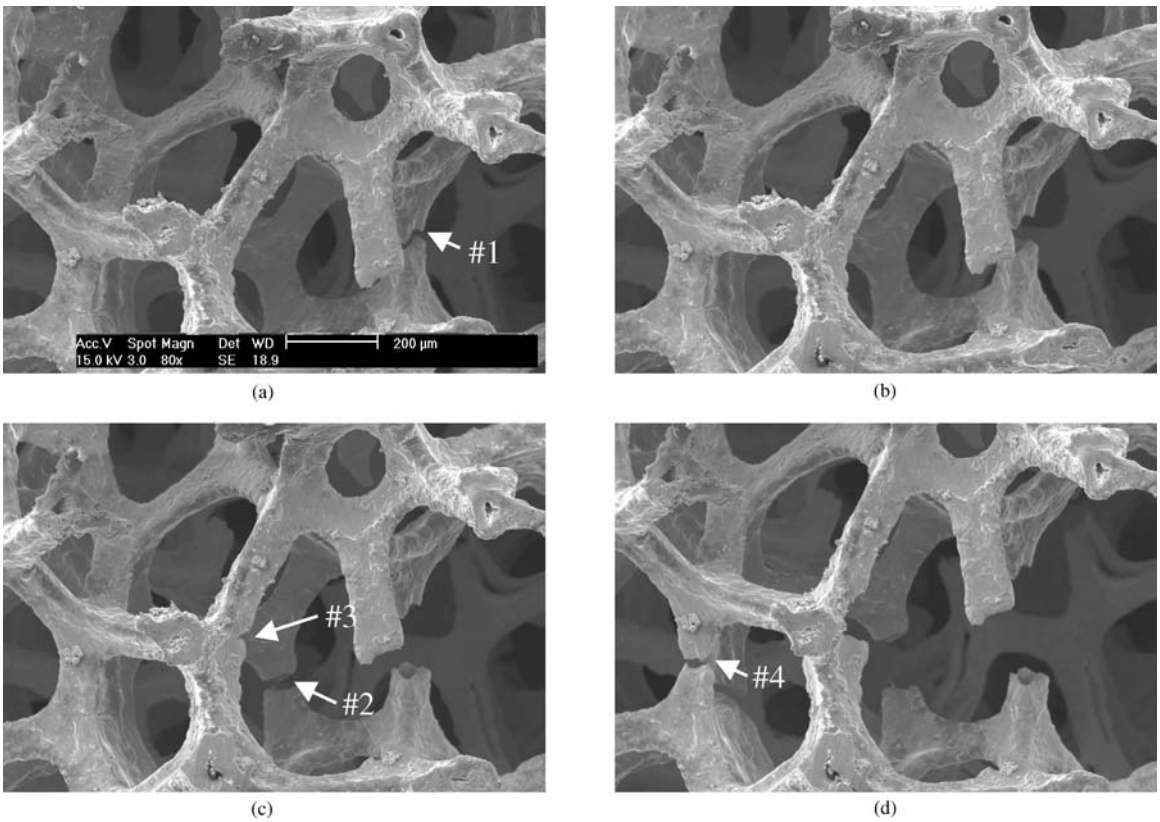

Figure 10 In-situ snapshots during damage development in the Recemat samples. The images (a) through (d) correspond to the instants depicted on the force-displacement curve of Fig. 9.

for the cracking process is that the intermediate struts remain in tact, bridging the main crack (see also [9, 10]). Final fracture occurs when the struts fail. Fig. 5a shows a BSE image of a representative part of the fracture surface. Two different regions can be identified: I ductile fracture due to void growth by plastic flow and II: brittle fracture due to cleavage of clustered precipitates. These precipitates were characterized in the previous subsection. When the precipitates cleave they effectively form penny-shaped cracks in an aluminium matrix. The penny-shaped cracks open up and grow by plastic flow of the surrounding aluminium matrix until they coalesce, leaving necking riches behind between the precipitates (see Fig. 5a). At some places on the fracture surface large holes were found, one order of magnitude larger than the dimples of the voids (see Fig. 5b). These holes were present from the onset, as shown in [3] and verified in the present study by means of a micro-CT scan of the undeformed material. A critical strain (at peak tensile load) of 1.5% was found.

3. Cymat foam

Cymat foam is manufactured using a melt gas injection technique (see Fig. 1b). First 5–15 wt% SiC particles are added to enhance the viscosity. Then, air is injected in the melt that forms the bubbles, which rise to the surface and start to drain. Finally the foam is removed by a conveyor belt and left to cool and solidify. For more details see [1, 11, 12].

3.1. Microstructural characterization

The Cymat foam analyzed here has a relative density in the range 0.03–0.2, a cell size ranging from 200 μm to 5 mm, a strut thickness of 100–500 μm and a cell wall thickness of 20–100 μm. The foam has a rather nonuniform cellular morphology with a clear directionality as a result of the manufacturing procedure. Fig. 6a shows a BSE image of a section of the foam, from which the SiC particles can be seen to concentrate at the surface of the solid material, resulting in a higher density of SiC in the cell walls compared to the struts. The diameter of the silicon carbide particles ranges from 5 to 25 mm. In the interior of the struts dendrites have formed with and interdendritic network of eutectic silicon (mostly) and Mg-Si-Fe-Cu needles (see Fig. 6b). The grain size was found to be in the range 20–100 mm. The above observations are in close agreement with findings elsewhere [3, 5, 14].

3.2. *In situ* fracture and fractography

In-situ fracture tests were performed, similar to the one outlined in Section 2.2. The dominant crack nucleates at the edge of the sample and spreads through the specimen identical to the process in Alporas (Fig. 4). Also here we found some struts bridging the cell wall cracks. The main difference with Alporas is that the process is more brittle; a critical strain of 0.5% was found for the Cymat foam. Fig. 7 shows a BSE image of a fracture surface of a cell wall. The surface contains SiC particles in between which Si and Mg-Si-Fe-Cu precipitates were found. There was no evidence of a ductile failure mechanism.

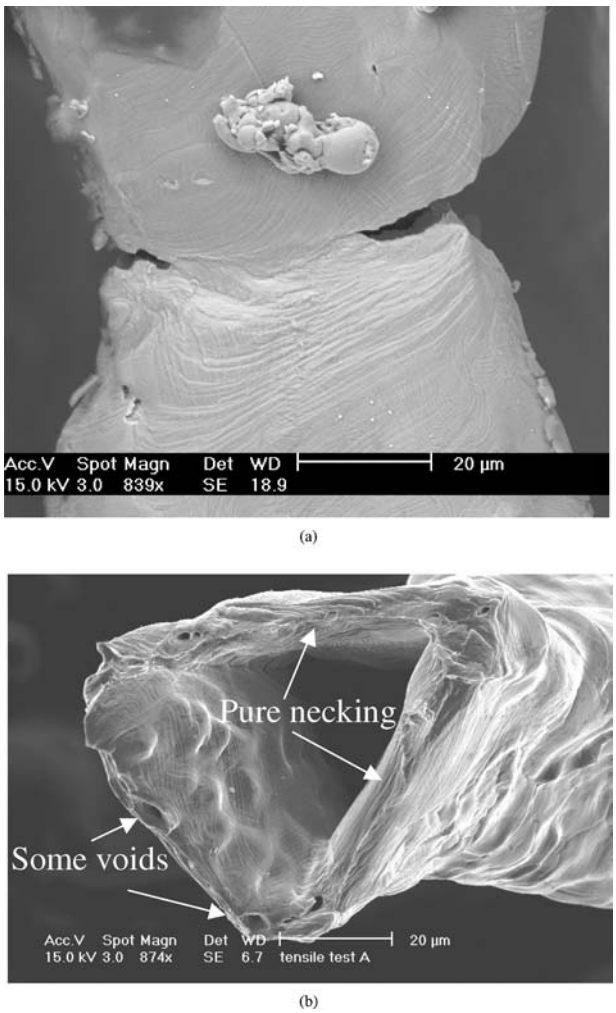

Figure 11 (a) In-situ SEM image of a failing strut (loading direction is vertical). (b) Fracture surface of a failed strut (viewing direction is parallel to the loading direction).

4. Recemat foam

Recemat foam is produced by an electrolytic process. First, a conductive layer is evaporated on the surface of a polyurethane open-cell foam. Then, the nickel chromium alloy is deposited through electroplating. Finally, the polymer preform is removed by a heat treatment, leaving behind a morphological copy of the polymer foam with hollow nickel chromium struts (see Fig. 1c).

4.1. Microstructural characterization

The Ni-Cr foam analyzed here (product specification RCM-NC-4753-05) has a chromium content between 20 and 40 wt%, a density of 0.60–0.65 g/cm^3, an observed cell size ranging from 300 to 500 μm, a strut thickness of approximately 75 μm and a strut wall thickness of approximately 20 μm. Fig. 8 shows a SEM-image of an etched cross-section of a strut, clearly highlighting that the struts are hollow and have a triangular cross-section, both being fingerprints of the

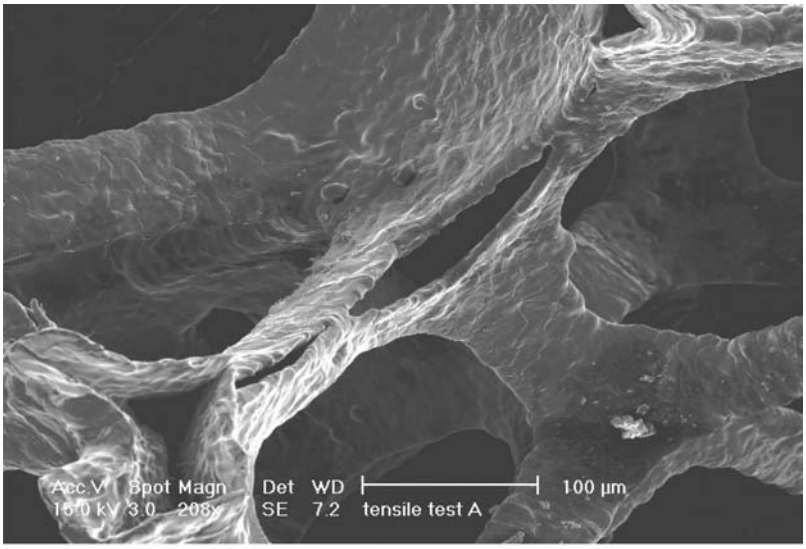

(a)

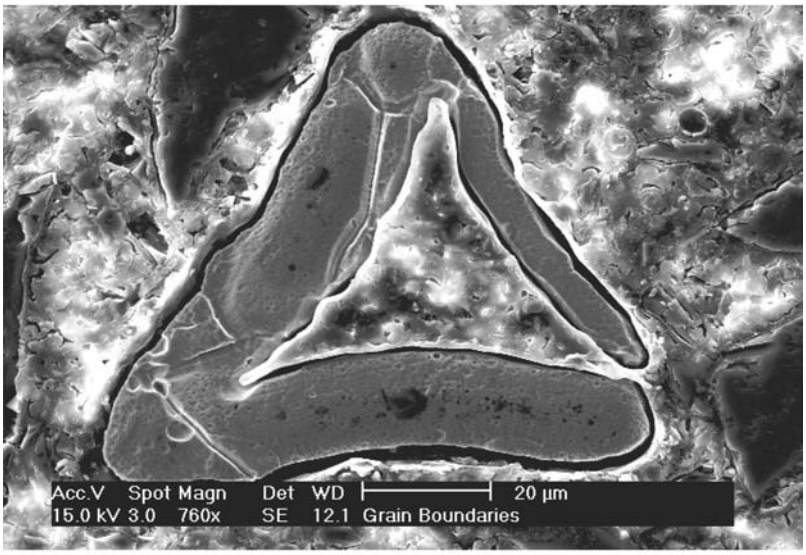

(b)

Figure 12 (a) SEM image of the fracture surface of Recemat foam showing unzipping of struts along the longitudinal axis. (b) Etched section through a Recemat strut, showing an initial imperfection.

polyurethane preform. The grains were found to have a long axis of 36 μm and a short axis of 12 μm on average. The strut walls are approximately one grain thick, which is in agreement with [15].

4.2. *In situ* fracture and fractography

Small samples of Recemat foam are tested *in situ*, where circular edge notches have been machined to ensure that damage development remains localized between the notches. The samples are 10 mm wide, 4 mm thick (giving a cross-sectional area $A = 40$ mm^2), 20 mm high and have a notch radius of 1.5 mm (Fig. 9). Note that here, in comparison to the Alporas and Cymat samples, there are approximately 18 cells between the notches, ensuring bulk properties to be measured. The force displacement curves of two tensile fracture tests are depicted in Fig. 9. The curves show an elastic region, a linear hardening regime, followed by failure at a normalized peak load of approximately 9 MPa at a critical strain of 8–9%. Four snapshots (denoted a–d) along the unloading branch of one of the curves are shown in Fig. 10. Fig. 10a corresponds to the moment of crack initiation in a strut (#1) adjacent to the right notch. In Fig. 10b the two parts of the struts separate until at instant c ($u/H = 8\%$) a second strut (#2) has failed (see Fig. 10c). Also visible in Fig. 10c is that at a third strut (#3) a surface crack has appeared due to the bending moment that developed due to opening of the failed region on the right hand side of the strut. In Fig. 10d struts #3 and #4 fail. One dominant crack forms, oriented perpendicular to the tensile direction spanning the region between the edge notches. Depending on the orientation of the struts with respect to the loading direction, the struts fail subject to uniaxial tension (e.g. struts #1, #2 and #4 in Fig. 10) or to uniaxial tension in combination with bending (strut #3 in Fig. 10). Fig. 11a shows a magnification of a strut failing in uniaxial tension photographed *in situ* (load direction is vertical). The picture clearly shows slip activity, leaving slip traces on the surface. Fig. 11b shows the fracture surface of a strut (viewing angle

oriented more or less along the longitudinal direction of the strut). The walls of the triangular strut have failed almost entirely by necking, although at some places one or two voids have formed prior to failure. The failure process is very ductile, with almost all energy dissipated through plastic deformation during necking. This is consistent with the initial microstructural characterization where no precipitates were found in the nickel chromium alloy.

Observation of the fracture surface yielded another damage mechanism: the unzipping of struts along the longitudinal axis (see Fig. 12a and the background of Fig. 10). This is probably related to imperfections in the strut wall microstructure at locations where grain boundaries are located at one of the three corners of the triangle in combination with a thin strut wall (see Fig. 12b). The small area of the grain boundary makes it susceptible to failure subject to shear forces that develop in the strut as a result of bending and torsion.

5. Concluding remarks

Three different metal foams were analyzed in a three-step process: (i) microstructural characterization, (ii) *in situ* fracture tests, (iii) fractography.

- Failure in the Alporas foam is initiated by cleavage/debonding of clustered precipitates (consisting of a combination of Ca, Ti and Fe) located around the grain boundaries. The ligaments between the failed precipitates rupture by void growth and coalescence. The origin of the precipitates' composition can be traced back to the Al alloy's composition and the manufacturing process, in which Ca was used for viscosity enhancement and TiH_2 as foaming agent.
- Failure in Cymat foam is caused by cleavage/debonding of SiC particles and interdendritic Si and Mg-Si-Cu-Fe precipitates. The SiC particles were added in the manufacturing process to ensure stability during drainage and solidification and the interdendritic precipitates resulted from the Al alloy composition during solidification.
- Failure in Recemat foam is initiated by the onset of necking in strut walls. No embrittling phases were found in the nickel chromium microstructure, resulting in a high ductility.

The results of this study can be used as a guide for improvement of closed-cell foam manufacturing procedures. The specific choice of Al alloy, viscosity enhancing additions and foaming agent should be made in light of the thermal history during foam solidification in order to control the physical microstructure of the cell walls and eliminate embrittling phases. The well-developed scientific literature on the physical metallurgy of casting alloys can be consulted to do so.

Acknowledgements

A.M. Harte (Cymat Aluminum Corperation) and H.A. Verduyn (Recemat International BV) are acknowledged for supplying the Cymat and Recemat foams, respectively.

References

1. M. F. ASHBY, A. G. EVANS N. A. FLECK, L. J. GIBSON, J. W. HUTCHINSON and H. G. WADLEY, *Metal Foams: A Design Guide* (Butterworth-Heinemann, 2000).
2. A.-M. HARTE, N. A. FLECK, and M. F. ASHBY, *ibid.* **47** (1999) 2511.
3. A. E. SIMONE, and L. J. GIBSON, *ibid.* **46** (1998) 3109.
4. A. E. MARKAKI and T. W. CLYNE, *ibid.* **49** (2001) 1677.
5. Y. SUGIMURA, J. MEYER, M. Y. HE, H. BART-SMITH, J. GRENESTEDT and A. G. EVANS, *ibid.* **45** (1997), 5245.
6. V. GERGERLY, H. P. DEGISCHER and T. W. CLYNE, *Comprehensive Composite Materials* **3** (2000) 1.
7. P. R. ONCK, E. W. ANDREWS and L. J. GIBSON, *ibid.* **43** (2001) 681.
8. E. W. ANDREWS, G. GIOUX, P. R. ONCK and L. J. GIBSON, *ibid.* **43** (2001) 701.
9. K. Y. G. MCCULLOUGH, N. A. FLECK and M. F. ASHBY, *ibid.* **4** (1999) 2331.
10. C. MOTZ and R. PIPPAN, *ibid.* **50** (2002) 2013.
11. J. BANHART, *Progr. Mater. Sci.* **46** (2001) 559.
12. H.-P. DEGISCHER and B. KRISZT, *Handbook of Cellular Metals: Production, Processing, Applications* (John Wiley & Sons, 2002).
13. J. BANHART, *JOM* **52** (2000), pp. 22–27.
14. O. PRAKASH, H. SANG and J. D. EMBURY, *Mater. Sci. Eng. A* **199** (1995) 195.
15. V. GOUSSERY, Y. BIENVENU, S. FOREST, A.-F. GOURGUES, C. COLIN and J.-D. BARTOUT, in *Cellular Metals; Manufacture, Properties and Applications*, edited by J. Banhart, N. Fleck and A. Mortensen (Verlag MIT Publishing, 2003) p. 419.

Received December 2004
and accepted April 2005